Interaction potential for indium phosphide: a molecular dynamics and first-principles study of the elastic constants, generalized stacking fault and surface energies

2009 J. Phys.: Condens. Matter 21 095002

(http://iopscience.iop.org/0953-8984/21/9/095002)

J. Phys.: Condens. Matter **21** (2009) 095002 (8pp) doi:10.1088/0953-8984/21/9/095002

Interaction potential for indium phosphide: a molecular dynamics and first-principles study of the elastic constants, generalized stacking fault and surface energies

Paulo Sergio Branicio[1], José Pedro Rino[2], Chee Kwan Gan[1] and Hélio Tsuzuki[2]

[1] Materials Theory and Simulation Laboratory, Institute of High Performance Computing, 1 Fusionopolis Way, #16-16 Connexis, 138632, Singapore
[2] Departamento de Física, Universidade Federal de São Carlos, Via Washington Luiz km 235, São Carlos, São Paulo, 13565-905, Brazil

Received 20 August 2008, in final form 16 December 2008
Published 29 January 2009
Online at stacks.iop.org/JPhysCM/21/095002

Abstract
Indium phosphide is investigated using molecular dynamics (MD) simulations and density-functional theory calculations. MD simulations use a proposed effective interaction potential for InP fitted to a selected experimental dataset of properties. The potential consists of two- and three-body terms that represent atomic-size effects, charge–charge, charge–dipole and dipole–dipole interactions as well as covalent bond bending and stretching. Predictions are made for the elastic constants as a function of density and temperature, the generalized stacking fault energy and the low-index surface energies.

(Some figures in this article are in colour only in the electronic version)

1. Introduction

Despite considerable work in the last few decades the detailed understanding of the properties and phases of III–V semiconductors remains a challenge to theorists and experimentalists. Theoretical modeling is a powerful tool to predict microscopic properties of the local atomic structure and its dynamic behavior. Accurate *ab initio* molecular dynamics calculations have been used to generate structural models for several semiconductors such as Si [1–3], GaAs [4, 5] and InP [6, 7]. *Ab initio* calculations are, however, computationally very demanding. Because of that the development of analytical potentials for InP and other III–V semiconductors is of great interest and several models have been recently elaborated [8–18]. The modeling of binary materials is, in fact, more difficult than that for single elements, such as Si and Ge, for which the Stillinger–Weber [19] and Tersoff [20] models work well. Models for these materials have to cope with the complexity posed by the presence of both covalent and partial ionic bonding. This work proposes an analytical interaction potential for InP that represents this complex bonding through many-body interactions.

InP, among other III–V semiconductors, is a very promising material for several applications such as optoelectronic devices, e.g. InP-based solar cells [21] and quantum-cascade lasers [22]. With advances in the synthesis of nanowires and nanoribbons, novel applications of InP-based devices have also been investigated such as photodetectors [23], flexible devices for wearable and disposable electronics [24] and polarized nanoscale light-emitting diodes [25].

Besides optoelectronics there is also considerable interest in the high pressure phases of InP. The reason is that, despite considerable work in the last few decades, the detailed understanding of the high pressure structures of InP and other semiconductors remains a challenge to theorists and experimentalists [26]. Early InP studies [27] found a semiconductor to metallic phase transition for InP. X-ray diffraction data showed that this transition is, in fact, a structural transformation from zinc blende to rock salt at 13.3 GPa [28]. *Ab initio* [29] and x-ray diffraction [30]

investigations confirmed this transition to occur at 10–10.8 GPa. At higher pressures the sequence of InP phases, up to 46 GPa, was shown to be zinc blende, rock salt and *Cmcm*-like [31]. Further transitions to *Immm* and CsCl structures were predicted [32, 33] even though no experiment has been performed to confirm them [26].

With the potential proposed here the high pressure phases of InP and the structural phase transition mechanisms were investigated using molecular dynamics (MD) simulations [34, 35]. The calculated sequence of high pressure phases is zinc blende, rock salt, rhombohedral and CsCl. The vibrational density of states of InP and its dependence on temperature and pressure were also characterized [36].

In this paper the parameters of the proposed InP interaction potential are presented and described in detail. The potential is validated by comparing calculated results with experimental and theoretical data. Predictions are made for the elastic constants, generalized stacking fault and surface energies and compared with first-principles calculations. This paper is divided into seven sections. In section 2 the interaction potential is described and the parameters for the two- and three-body terms are provided. In sections 3 and 4 results are presented and compared with available experimental and theoretical data. The results are divided into structural energies (section 3); surfaces and generalized stacking fault energies (section 4); thermal properties (section 5); and elastic properties (section 6). Conclusions are summarized in section 7.

2. Interaction potential model

The interaction model for InP proposed here is based on the model developed by Vashishta *et al* [37] to describe semiconductors and ceramic materials. The functional form of the potential consists of two- and three-body terms, representing several physical interactions among atoms:

$$U = \sum_{i<j}^{N} U_{ij}^{(2)}(r_{ij}) + \sum_{\substack{i,j<k \\ j\neq i,k\neq i}}^{N} U_{ijk}^{(3)}(\vec{r}_{ij}, \vec{r}_{ik}), \tag{1}$$

where N is the number of atoms, $\vec{r}_i$ is the position of the ith atom, $\vec{r}_{ij} = \vec{r}_i - \vec{r}_j$, and $r_{ij} = |\vec{r}_{ij}|$.

The chemical bonds in InP and other III–V semiconductors have both ionic and covalent features. When InP is formed charge is transferred between In and P atoms, resulting in a Coulomb interaction between the ions. Atoms also interact by charge-induced dipole and dipole–dipole (van der Waals) interactions, arising from the electronic polarizability of the ions. At short range atoms repel each other due to the Pauli exclusion principle. The two-body term of the effective interaction potential representing all these two-body interactions is given by

$$U_{ij}^{(2)}(r) = \frac{H_{ij}}{r^{\eta_{ij}}} + \frac{Z_i Z_j}{r} e^{-r/\lambda_1} - \frac{D_{ij}}{r^4} e^{-r/\lambda_4} - \frac{w_{ij}}{r^6}, \tag{2}$$

where H_{ij} is the strength of the short range steric repulsion, $r \equiv r_{ij}$, η_{ij} are the exponents of the steric repulsion term, Z_i the effective charge, D_{ij} the strength of the charge–dipole attraction, w_{ij} the van der Waals interaction strength, and λ_1 and λ_4 are the screening lengths for Coulomb and charge–dipole terms, respectively.

The strengths of the steric repulsion, H_{ij}, and charge–dipole interactions, D_{ij}, for the pair of atoms i and j are estimated from

$$H_{ij} = A\left(\sigma_i + \sigma_j\right)^{\eta_{ij}} \tag{3}$$

and

$$D_{ij} = \frac{\alpha_i Z_j^2 + \alpha_j Z_i^2}{2}, \tag{4}$$

where A is the repulsion strength while σ_i and α_i are the ionic radius and the electronic polarizability of the ith atom, respectively.

For computational efficiency the screening lengths were fixed at $\lambda_1 = 4.5$ Å and $\lambda_4 = 2.75$ Å and the two-body interaction is truncated at $r = r_c = 6.0$ Å. For $r < r_c$ the potential is shifted to make the potential and its first derivative continuous at r_c [38]. The expression for the shifted two-body potential is

$$U_{ij}^{(2)}(r)_{\text{shifted}} = \begin{cases} U_{ij}^{(2)}(r) - U_{ij}^{(2)}(r_c) - (r - r_c) \\ \qquad \times \left(\mathrm{d}U_{ij}^{(2)}(r)/\mathrm{d}r\right)_{r=r_c} & r \leqslant r_c \\ 0 & r > r_c. \end{cases} \tag{5}$$

However, two-body interactions are not sufficient to describe the effects of all interactions in InP. An addition three-body potential is needed to describe the covalent character of bond bending and stretching. Stillinger and Weber [19] proposed a three-body term to account for the short range order in a tetrahedrally coordinated covalent material. The three-body term proposed here for InP has a significant modification that is necessary to describe the melting and the several structural transformations under pressure. At the same time it continues to describe the bond bending and bond stretching of the covalent bonds in the low pressure phase. The proposed three-body potential has spatial and angular dependence defined by

$$U_{ijk}^{(3)}(\vec{r}_{ij}, \vec{r}_{ik}) = \Gamma(r_{ij}, r_{ik})\Lambda(\theta_{jik}), \tag{6}$$

where

$$\Gamma(r_{ij}, r_{ik}) = B_{jik} \exp\left(\frac{\gamma}{r_{ij} - r_0} + \frac{\gamma}{r_{ik} - r_0}\right) \times \Theta(r_0 - r_{ij})\Theta(r_0 - r_{ik}), \tag{7}$$

and

$$\Lambda(\theta_{jik}) = \frac{(\cos\theta_{jik} - \cos\theta_0)^2}{1 + C\,(\cos\theta_{jik} - \cos\theta_0)^2}. \tag{8}$$

Here B_{jik} is the strength of the three-body interaction, θ_{jik} the angle formed by $\vec{r}_{ij}$ and $\vec{r}_{ik}$, θ_0 the covalent bond angle, C the three-body saturation parameter and $\Theta(r_0 - r_{ij})$ the step function defined by

$$\Theta(x) = \begin{cases} 1 & x \leqslant 0 \\ 0 & x > 0. \end{cases} \tag{9}$$

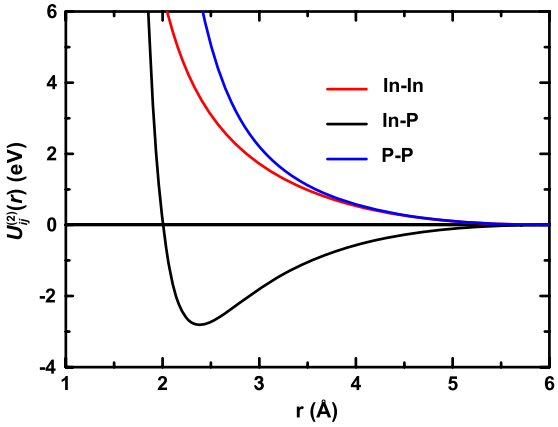

Figure 1. Two-body interaction term of the potential, see equation (5), as a function of distance for In–In, In–P and P–P pairs.

Table 1. The parameters of the InP interaction potential. Length, energy and charge units are Å, J and electron charge, respectively. Z is the effective ionic charge, α the electronic polarizability and σ the ionic radius. η is the steric repulsion exponent and w the van der Waals strength. B is the three-body strength. λ_1 and λ_4 are the screening lengths for Coulomb and charge–dipole interactions, while r_c is the two-body cutoff radius, A the repulsion strength, and r_0, γ, θ_0 and C are the three-body range, exponent, bond angle and saturation parameter, respectively.

	Z (e)	α (Å^3)	σ (Å)
In	1.21	0.0	1.1
P	−1.21	2.5	1.4412
	η	w (J Å^6)	
In–In	7.0	0.0	
In–P	9.0	43.276×10^{-18}	
P–P	7.0	0.0	
	B (J)		
In–P–In	6.969×10^{-19}		
P–In–P	6.969×10^{-19}		
λ_1 (Å)	4.5		
λ_4 (Å)	2.75		
r_c (Å)	6.0		
A (J)	1.7573×10^{-19}		
r_0 (Å)	3.55		
γ (Å)	1.0		
θ_0 (deg)	109.47		
C	7.0		

The short range three-body interaction has $r_0 = 3.55$ Å and $\gamma = 1$ Å. For InP, θ_0 is the tetrahedral angle 109.47°.

Variations of this interaction potential model were successfully used to study a number of materials such as SiO_2 [37, 39], Si_3N_4 [40–42], GaAs [8, 9], SiC [43–45], CaO [46], AlN [47, 48] and Al_2O_3 [49, 50].

In this work the parameters of the proposed model are optimized to reproduce an extended experimental dataset of InP. The fitting database includes the lattice constant, cohesive energy, melting temperature, bulk modulus, and the C_{11} and C_{12} elastic constants in the zinc blende structure. Table 1 summarizes the fitted parameters.

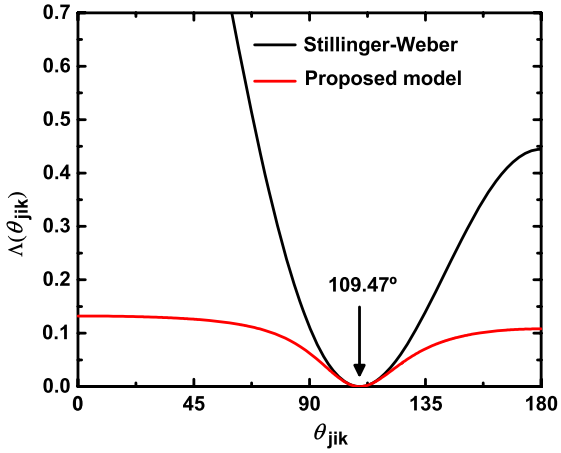

Figure 2. Angular dependence of the three-body interaction potential defined in equation (8). For comparison the Stillinger–Weber three-body interaction potential is also displayed. In this plot $\theta_0 = 109.47°$ and $C = 7$, as given in table 1.

Table 2. Theoretical and experimental values of selected InP properties.

		Experiments	MD
Lattice constant (Å)		5.87 [51]	5.869
Cohesive energy (eV)		−3.34 [63], −3.48 [64]	−3.48
Melting temperature (K)		1331 [65]	1229
Zinc blende to rock salt transition pressure (GPa)		10–13.3 [27–30]	10 [34, 35]
Bulk modulus (GPa)		71.1 [66], 72.5 [67]	72.3
Elastic constants	C_{11} (GPa)	101.1 [66], 102.2 [67]	102.5
	C_{12} (GPa)	56.1 [66], 57.6 [67]	57.3
	C_{44} (GPa)	45.6 [66], 46.0 [67]	69.6

Figure 1 shows the shifted $U_{ij}^{(2)}(r)$ interaction potential as a function of distance for In–In, In–P and P–P pairs. The angular term of the three-body interaction potential Λ is shown in figure 2. Note that in the Stillinger–Weber model the angular dependence makes the potential energy increase drastically when the angle deviates from the equilibrium value. In the proposed model the potential energy saturates for large deviations, but keeps the same dependence around the equilibrium angle. This allows for the reconfiguration of bonds in InP structural transformations under pressure and during melting. Table 2 summarizes some quantities that have been calculated using the proposed interaction potential and the corresponding experimental data. The length scale has a numerical accuracy of 0.005 Å, which is defined by the histogram definition in our code, energy has an accuracy of 0.01 eV/particle, melting temperature error is ±56 K and elastic constant accuracy is 0.1 GPa.

3. Structural energies

The energy of the zinc blende InP structure calculated as a function of the volume is shown in figure 3(a). The curve can be used to predict the energy at equilibrium, the lattice constant, the bulk modulus and its derivative. Energetic curves

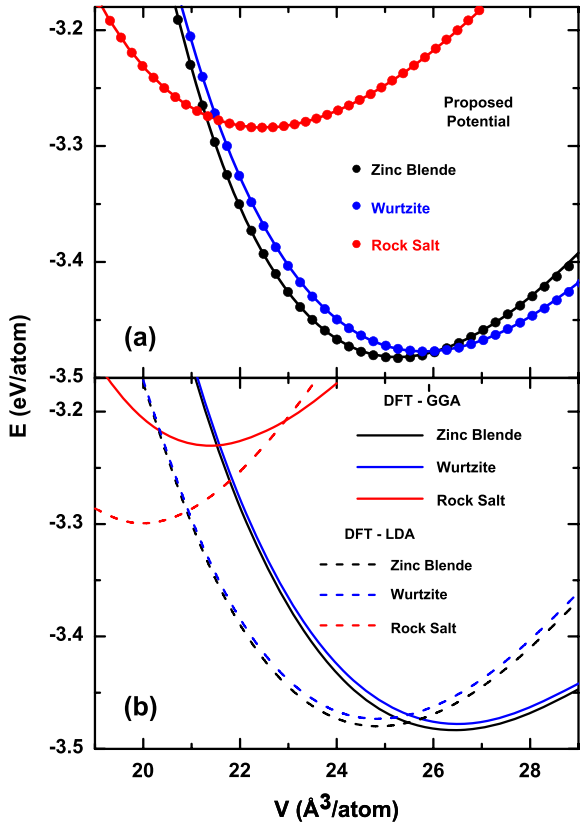

Figure 3. Energy of various InP structures as a function of volume. (a) Results obtained using the proposed potential for the zinc blende, rock salt and wurtzite structures. Lines connecting points are fittings of the Murnaghan equation of state. Zinc blende structure has the minimum energy at $E = -3.4828$ eV/atom with $V_0 = 25.2657$ Å^3/atom. The corresponding lattice parameter is $a_0 = 5.8687$ Å. The difference between wurtzite and zinc blende energy minima is $E = 0.0057$ eV. (b) Curves calculated using the density-functional theory (DFT) within the local density (LDA) and generalized gradient approximations (GGA).

for the wurtzite and rock salt structures were also calculated and are displayed in figure 3(a). It can be seen that the zinc blende structure is the most stable structure for InP. The small positive difference between wurtzite and zinc blende energy minima, $\Delta E = 0.0057$ eV, indicates a positive stacking fault energy. These static calculations were done with a system of 500 In and 500 P atoms in a cubic MD box. To change the volume the system was equally scaled in the x, y and z directions. The equilibrium energy of the zinc blende structure indicates a lattice parameter of 5.8687 Å, in agreement with the experimental value of 5.87 Å [51]. The energetic curves of zinc blende and rock salt phases are also presented in [34] as well as energetic curves for other high pressure phases of InP up to 100 GPa. The different structural transitions among these phases are discussed in [35].

To evaluate the accuracy of the curves in figure 3(a) the energy–volume curves for zinc blende, wurtzite and rock salt structures were also calculated with the density-functional theory (DFT) method [52, 53] implemented in the Vienna *ab initio* simulation package (VASP) [54]. This package is used for all DFT calculations carried out in this work. Figure 3(b) shows the energetic curves calculated with both the local density approximation (LDA) and the generalized gradient approximation (GGA) for the exchange–correlation energy. Ultrasoft pseudopotentials [55] for In and P have been used, where the 4d states for In were included as valence electrons. A consistent high cutoff energy of 217 eV was used. That corresponds to a high precision setting in the VASP code which is suitable for describing the ultrasoft pseudopotential of In and P. The cutoff energy was evaluated to make sure it is sufficient for this study. The Monkhorst–Pack scheme [56] was used for the k-point sampling in the reciprocal space. The k-point mesh is chosen in such a way that total energy convergence of a few meV/atom is achieved. For ease of comparison, the curves in figure 3(b) have been shifted in such a way that the minimum energy coincides with that obtained using the proposed interaction potential. The order of stability of the three curves agrees well with that obtained with the potential. At low densities (under tension) the interaction potential predicts the wurtzite structure to be more stable than the zinc blende structure. However, DFT results indicate that the zinc blende structure is always more stable than the wurtzite structure within the density range we have considered. The minima energy of the zinc blende curves indicates lattice parameters of 5.96 Å, with GGA, and 5.84 Å, with LDA. The value obtained using LDA is closer to that obtained using the potential which is in agreement with the experimental value.

Table 3. Parameters of the Murnaghan equation of state fitted to the energetic curves for the zinc blende, wurtzite and rock salt structures shown in figure 3. E/N is the minimum energy per atom, V/N the minimum volume per atom, B the bulk modulus and B' the first pressure derivative of B.

		Murnaghan equation of state
Zinc blende	E/N (eV)	−3.482
	V/N (Å^3)	25.3
	B (GPa)	70.5
	B'	5.88
Wurtzite	E/N (eV)	−3.477
	V/N (Å^3)	25.81
	B (GPa)	60.88
	B'	5.195
Rock salt	E/N (eV)	−3.28
	V/N (Å^3)	22.47
	B (GPa)	49.85
	B'	4.51

For each of the energetic curves in figure 3(a) a Murnaghan equation of state was fitted to the data. The resulting curves are shown as continuous lines connecting the calculated points in figure 3(a). This equation is defined by

$$E(V) = \frac{BV}{B'(B'-1)}\left[B'\left(1-\frac{V_0}{V}\right)+\left(\frac{V_0}{V}\right)^{B'}-1\right]+E(V_0). \tag{10}$$

The fitted parameters with a standard deviation of less than 10^{-5} are shown in table 3 for zinc blende, wurtzite and rock salt structures.

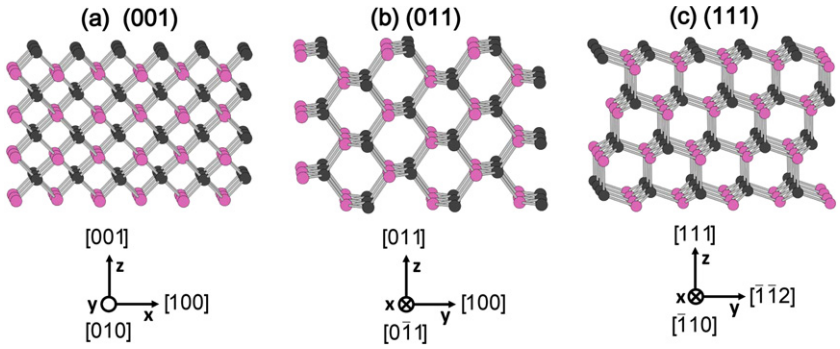

Figure 4. Schematics of the InP (a) (001), (b) (011) and (c) (111) unreconstructed surfaces given by top and bottom atomic layers. Structures are slightly tilted from the direction alignment indicated in order to highlight the structure of the surfaces.

Table 4. Unrelaxed and relaxed InP surface energies for the low-index (001), (011) and (111) planes.

Surface	(001)	(011)	(111)
Unrelaxed (J m^{-2})	1.46	0.63	0.67
Relaxed (J m^{-2})	1.39	0.60	0.59
DFT-LDA (J m^{-2})	1.88	0.79	1.44

4. Surfaces and generalized stacking fault energies

InP unreconstructed surface energies were calculated for the three low-index (001), (011) and (111) planes illustrated in figure 4. Three different unit cells were used to create orthogonal systems with these surfaces perpendicular to the z direction. The total energy of the system was calculated for the bulk, where periodic boundary conditions were applied in all directions to avoid surface effects. The system energy was recalculated with two vacuum regions added above and below the original InP system in the z direction. The energy was calculated with and without surface relaxation. The energy difference between the bulk and vacuum set-ups provides the surface energies of the system. For unrelaxed and relaxed surfaces, the surface energies are given by table 4. To the best of the author's knowledge there is no experimental result available for these quantities. However, for comparison DFT-LDA calculations, using the VASP package [54], of the surface energies are also shown in table 4. The energies for the non-polar (011) surface have the best agreement. In DFT calculations, the atomic structure of slab models is fully relaxed. The models are constructed out of bulk configurations obtained in the calculations described in section 3. A relatively large vacuum layer of 12 Å is used throughout the calculations. The k-point meshes for the (001), (011) and (111) surface energy calculations are $5 \times 5 \times 1$, $6 \times 6 \times 1$ and $6 \times 6 \times 1$, respectively. The number of atomic layers for (001), (011) and (111) surfaces are 12, 12 and 18, respectively. This corresponds to 24-atom, 24-atom and 18-atom supercells.

The energy barrier for plastic deformations in InP is estimated by calculating the generalized stacking fault energy for rigid shear of the (111) gliding plane of the zinc blende structure by both MD and DFT-LDA methods. The generalized stacking fault energy calculation procedure follows that of Tadmor and Hai [57] adapted to the zinc blende crystal. A

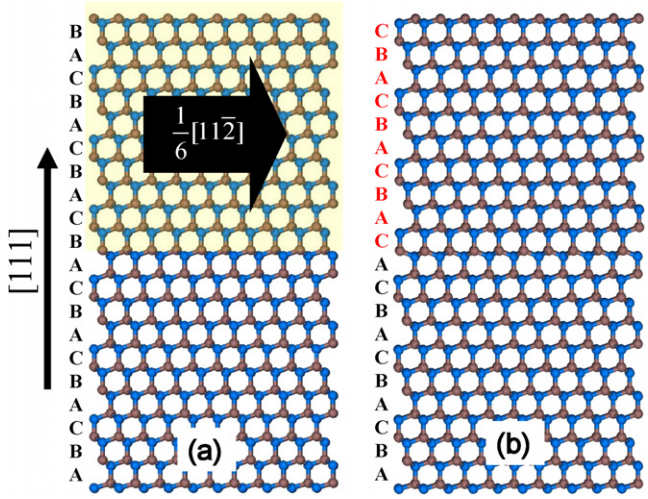

Figure 5. InP crystal system used for rigid sliding along the [$\bar{1}$10] direction. The right panel shows the final slid system with an intrinsic stacking fault created.

bulk single-crystal sample with 42 atomic layers in the ⟨111⟩ direction was created. Vacuum layers were added above and below the system in the ⟨111⟩ direction, creating (111) surfaces that were relaxed for 10 000 Δt (one time step $\Delta t = 5.0$ fs). The relaxation was achieved by quenching the temperature to 0 K by scaling the velocities by a factor of 0.7 every $10\Delta t$. The top 21 layers of the system were then rigidly sheared against the remaining 21 layers, on the (111) glide plane in the ⟨11$\bar{2}$⟩ direction using 100 steps forming an intrinsic stacking fault, see figure 5. Each atomic configuration generated during the shearing was relaxed for $10\,000\Delta t$ in the ⟨111⟩ perpendicular direction, in order to get a minimum energy configuration. The energetics of the rigid shearing shows good agreement between MD and DFT-LDA results as shown in figure 6. The value of the unstable stacking fault energy is 54 meV Å^{-2} (MD) and 72 meV Å^{-2} (DFT-LDA), while the intrinsic stacking fault energy is 1.41 meV Å^{-2} (MD) and 1.47 meV Å^{-2} (DFT-LDA). The intrinsic stacking fault energy predicted with the proposed potential is in reasonable agreement with reported experimental values of 0.9 meV Å^{-2} [58] and 1.1 meV Å^{-2} [59].

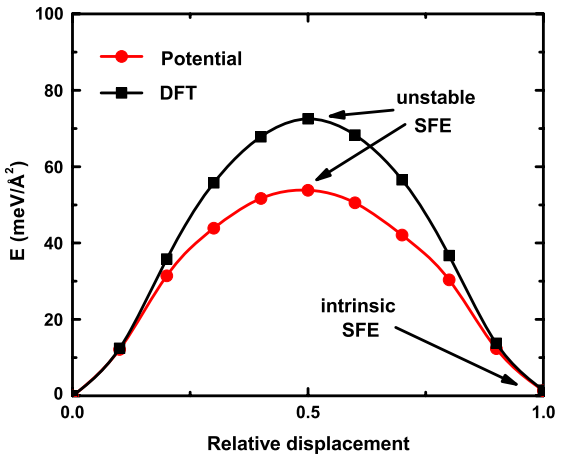

Figure 6. Generalized stacking fault energy curve for InP using the proposed potential and DFT-LDA. For both methods the potential energy is shown for rigid sliding along the $[11\bar{2}]$ direction until an intrinsic stacking fault is formed. The calculated unstable and intrinsic stacking fault energies from potential (DFT-LDA) are 54 (72) meV Å^{-2} and 1.41 (1.47) meV Å^{-2}.

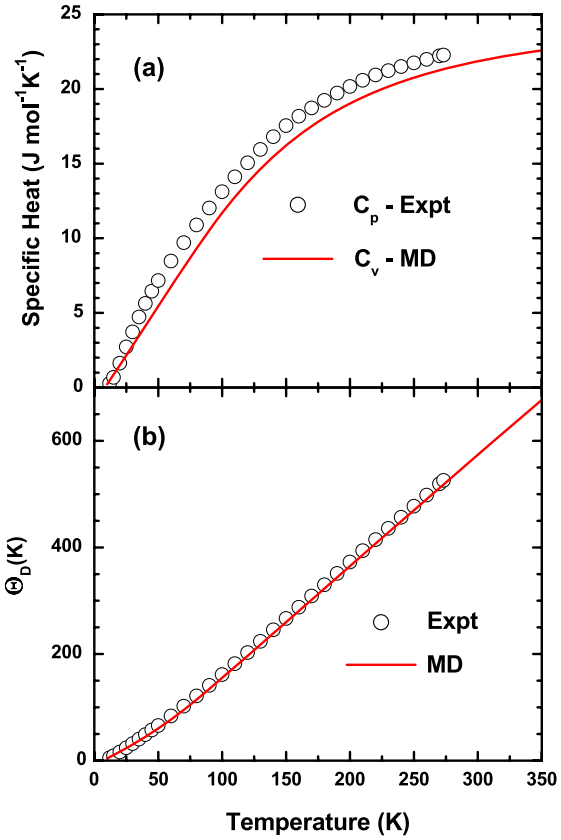

Figure 7. (a) Temperature dependence of the InP specific heat, calculated from MD at constant volume, C_V, and measured at constant pressure, C_P. (b) Low temperature limit of the Debye temperature calculated from the data in (a).

5. Thermal properties

From the knowledge of the InP vibrational density of states [36], $G(\omega)$, the heat capacity at constant volume can be evaluated by

$$C_V = \frac{3Nk_B \int_0^\infty \frac{u^2 e^u}{(e^u-1)^2} G(\omega)\, d\omega}{\int_0^\infty G(\omega)\, d\omega},$$

where $u = \hbar\omega/k_B T$ and k_B is the Boltzmann constant. Figure 7(a) displays the calculated C_V as a function of temperature along with the experimental values of C_P [60, 61]. The difference between C_P and C_V can be estimated from $\Delta C = C_P - C_V = 9TV\alpha^2 B_T$, where V, α and B_T are the volume, linear thermal expansion coefficient and isothermal bulk modulus, respectively. Considering that at $T = 273$ K $\Delta C = 0.7$ J mol^{-1} K^{-1} the curves have excellent agreement [61]. From the curves in figure 7(a) the Debye temperature Θ_D can be calculated from the low temperature expression $C_V = \frac{12}{5}\pi^4 N k_B (\frac{T}{\Theta_D})^3$. Figure 7(b) shows the calculated values of Θ_D as a function of temperature. At $T = 273$ K, $\Theta_D = 523$ K, from both experimental and MD data.

The melting temperature was calculated by slowly heating the system until the molten state was achieved. The molten state was prepared by heating the InP crystalline structure,

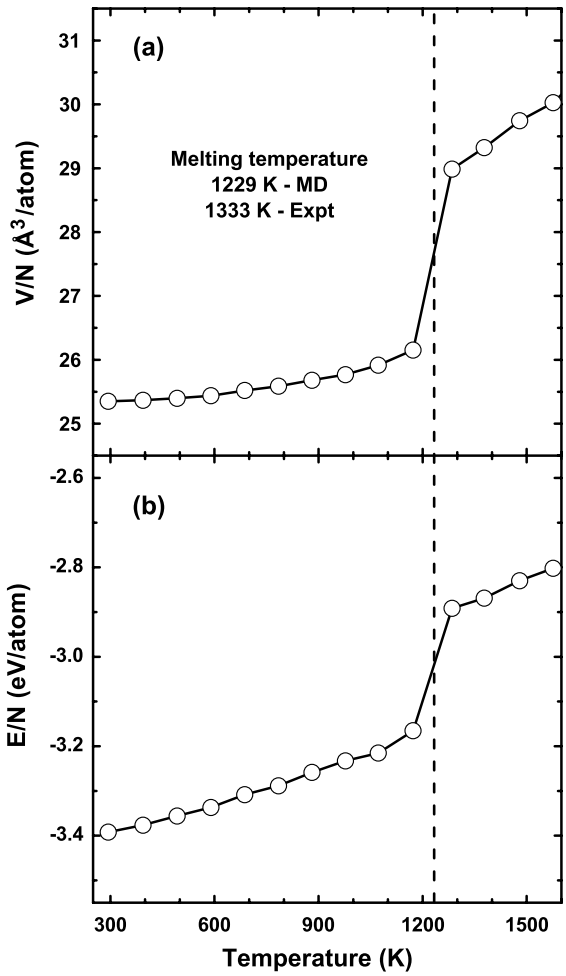

Figure 8. (a) Volume per atom and (b) energy per atom as a function of temperature. Solid lines connecting points are a guide to the eyes. Vertical dashed line indicates the calculated melting point at 1229 ± 56 K.

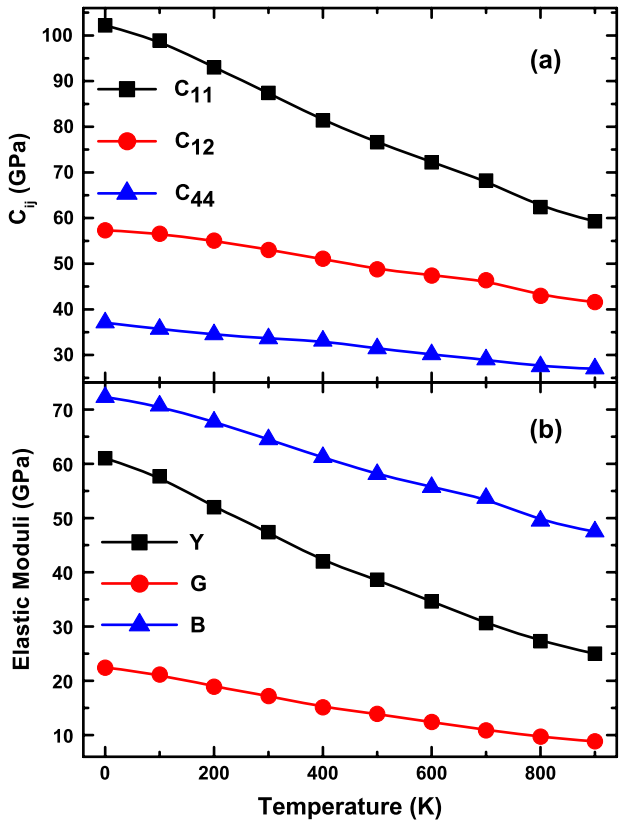

Figure 9. Calculated elastic properties of InP as a function of temperature. (a) Elastic constants C_{11}, C_{12} and C_{44}. (b) Young modulus, Y, shear modulus, G, and bulk modulus, B.

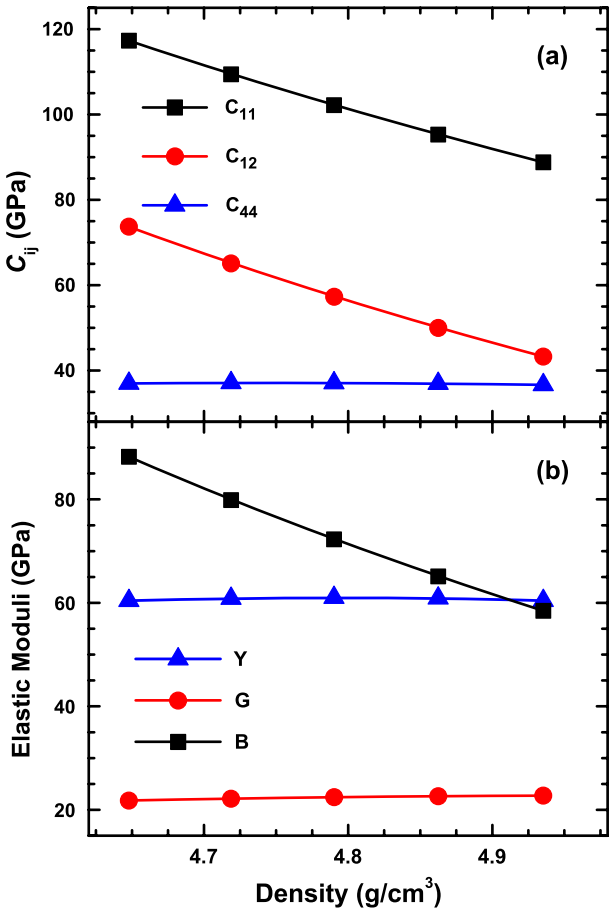

Figure 10. Calculated elastic properties of InP as a function of density. (a) Elastic constants C_{11}, C_{12} and C_{44}. (b) Young modulus, Y, shear modulus, G, and bulk modulus, B.

using the constant-pressure, constant-temperature MD method. Starting from its zinc blende structure at 300 K the system was heated in steps of about 100 K at constant $P = 0$ GPa. At each temperature, the system was thermalized for $30\,000\Delta t$. Averages of energy, volume and correlation functions were calculated over an additional $30\,000\Delta t$ in the equilibrium state.

In figures 8(a) and (b) the volume per atom and the energy per atom are displayed as a function of temperature. Between the temperatures 1173 and 1285 K a discontinuous increase in the volume and energy per atom indicates the melting of the system. The ensemble average temperature at these two points gives an estimated melting temperature of 1229 ± 56 K. This value is indicated by the vertical line in figures 8(a) and (b) and agrees well with the reported experimental melting temperature of 1331 K.

6. Elastic properties

As is shown in table 2, InP elastic constants were calculated for the zinc blende structure and agree well with experimental data. The elastic constants were calculated using the proposed interaction potential at zero temperature directly from the stress–strain relationship, i.e. $C_{\alpha,\beta,\mu,\nu} = \partial\sigma_{\alpha,\beta}/\partial\varepsilon_{\mu,\nu}$, where σ is the external applied stress and ε the strain [62].

The dependence of the elastic constants with temperature is shown in figure 9(a). From the data in that figure the most common elastic moduli, i.e. Young modulus, shear modulus and bulk modulus, were calculated and are plotted in figure 9(b). The Young modulus was determined through $Y = (C_{11} + 2C_{12})(C_{11} - C_{12})/(C_{11} + C_{12})$, shear modulus by $G = Y/[2(1+\nu)]$, with $\nu = C_{12}/(C_{11}+C_{12})$, and the bulk modulus by $B = Y/[3\,(1-2\nu)]$. All elastic constants and elastic moduli are softened at high temperatures and monotonically decay in the range 0–900 K.

At zero temperature the dependence of the elastic constants with density was calculated and is shown in figure 10(a). The Young, shear and bulk moduli are shown in figure 10(b). Within 1% density variation the bulk modulus shows a strong dependence with density. However the Young modulus and shear modulus are nearly independent of density in this range.

7. Conclusions

In summary the structural, elastic, thermal and surface properties of indium phosphide are investigated using MD simulations and DFT calculations. MD simulations use a proposed potential which is validated by a selected dataset of experimental properties. Predictions are made for the elastic constants as a function of density and temperature. Additional joint predictions using DFT are made for the unreconstructed

surface energies and the generalized stacking fault curve. As demonstrated by the results described throughout the text, the proposed potential has a wide range of applicability. However, application of this model to describe surface reconstruction processes and to characterize the properties of the high pressure, liquid and amorphous phases should be done with caution since the potential is not fitted to describe elemental bonds and higher coordination.

Acknowledgments

JPR and HT acknowledge support by FAPESP (Fundação de Amparo à Pesquisa do Estado de São Paulo, SP-Brazil) and CNPq (Conselho Nacional de Desenvolvimento Científico e Tecnológico–Brazil).

References

[1] Car R and Parrinello M 1988 *Phys. Rev. Lett.* **60** 204
[2] Sugino O and Car R 1995 *Phys. Rev. Lett.* **74** 1823
[3] Silvestrelli P L, Alavi A, Parrinello M and Frenkel D 1996 *Phys. Rev. Lett.* **77** 3149
[4] Difelice R, Shkrebtii A I, Finocchi F, Bertoni C M and Onida G 1993 *J. Electron. Spectrosc. Relat. Phenom.* **64/65** 697
[5] Godlevsky V V, Derby J J and Chelikowsky J R 1998 *Phys. Rev. Lett.* **81** 4959
[6] Srivastava G P 1994 *Surf. Sci.* **309** 328
[7] Gayathri N, Izvekov S and Voth G A 2002 *J. Chem. Phys.* **117** 872
[8] Branicio P S, Kalia R K, Nakano A, Rino J P, Shimojo F and Vashishta P 2003 *Appl. Phys. Lett.* **82** 1057
[9] Branicio P S, Rino J P, Shimojo F, Kalia R K, Nakano A and Vashishta P 2003 *J. Appl. Phys.* **94** 3840
[10] Akiyama T, Sano K, Nakamura K and Ito T 2006 *Japan. J. Appl. Phys.* 2 **45** L275
[11] Albe K, Nordlund K, Nord J and Kuronen A 2002 *Phys. Rev.* B **66** 035205
[12] Erhart P and Albe K 2005 *Phys. Rev.* B **71** 035211
[13] Gao F and Weber W J 2002 *Nucl. Instrum. Methods* B **191** 504
[14] Murdick D A, Zhou X W, Wadley H N G, Nguyen-Manh D, Drautz R and Pettifor D G 2006 *Phys. Rev.* B **73** 045206
[15] Nord J, Albe K, Erhart P and Nordlund K 2003 *J. Phys.: Condens. Matter* **15** 5649
[16] Oleinik I I and Pettifor D G 1999 *Phys. Rev.* B **59** 8500
[17] Pettifor D G and Oleinik I I 1999 *Phys. Rev.* B **59** 8487
[18] Pettifor D G and Oleinik I I 2000 *Phys. Rev. Lett.* **84** 4124
[19] Stillinger F H and Weber T A 1985 *Phys. Rev.* B **31** 5262
[20] Tersoff J 1989 *Phys. Rev.* B **39** 5566
[21] Coutts T J and Naseem S 1985 *Appl. Phys. Lett.* **46** 164
[22] Mujagic E, Austerer M, Schartner S, Nobile M, Hoffmann L K, Schrenk W, Strasser G, Semtsiv M P, Bayrakli I, Wienold M and Masselink W T 2008 *J. Appl. Phys.* **103** 033104
[23] Wang J F, Gudiksen M S, Duan X F, Cui Y and Lieber C M 2001 *Science* **293** 1455
[24] Duan X F, Niu C M, Sahi V, Chen J, Parce J W, Empedocles S and Goldman J L 2003 *Nature* **425** 274
[25] Gudiksen M S, Lauhon L J, Wang J, Smith D C and Lieber C M 2002 *Nature* **415** 617
[26] Mujica A, Rubio A, Munoz A and Needs R J 2003 *Rev. Mod. Phys.* **75** 863
[27] Minomura S and Drickamer H G 1962 *J. Phys. Chem. Solids* **23** 451
[28] Jamieson J C 1963 *Science* **139** 845
[29] Soma T, Satoh J and Matsuo H 1982 *Solid State Commun.* **42** 889
[30] Menoni C S and Spain I L 1987 *Phys. Rev.* B **35** 7520
[31] Nelmes R J, McMahon M I and Belmonte S A 1997 *Phys. Rev. Lett.* **79** 3668
[32] Mujica A and Needs R J 1997 *Phys. Rev.* B **55** 9659
[33] Mujica A and Needs R J 1997 *Phys. Rev.* B **56** 12653
[34] Branicio P S, Rino J P and Shimojo F 2006 *Appl. Phys. Lett.* **88** 161919
[35] Rino J P and Branicio P S 2007 *Phys. Status Solidi* b **244** 239
[36] Branicio P S and Rino J P 2007 *Phys. Status Solidi* b **244** 331
[37] Vashishta P, Kalia R K, Rino J P and Ebbsjo I 1990 *Phys. Rev.* B **41** 12197
[38] Allen M P and Tildesley D J 1987 *Computer Simulation of Liquids* (New York: Clarendon) p xix (Oxford: Oxford University Press)
[39] Campbell T, Kalia R K, Nakano A, Shimojo F, Tsuruta K, Vashishta P and Ogata S 1999 *Phys. Rev. Lett.* **82** 4018
[40] Loong C K, Vashishta P, Kalia R K and Ebbsjo I 1995 *Europhys. Lett.* **31** 201
[41] Nakano A, Kalia R K and Vashishta P 1995 *Phys. Rev. Lett.* **75** 3138
[42] Vashishta P, Kalia R K and Ebbsjo I 1995 *Phys. Rev. Lett.* **75** 858
[43] Shimojo F, Ebbsjo I, Kalia R K, Nakano A, Rino J P and Vashishta P 2000 *Phys. Rev. Lett.* **84** 3338
[44] Chatterjee A, Kalia R K, Nakano A, Omeltchenko A, Tsuruta K, Vashishta P, Loong C K, Winterer M and Klein S 2000 *Appl. Phys. Lett.* **77** 1132
[45] Vashishta P, Kalia R K, Nakano A and Rino J P 2007 *J. Appl. Phys.* **101** 103515
[46] Mota R C, Branicio P S and Rino J P 2006 *Europhys. Lett.* **76** 836
[47] Branicio P S, Kalia R K, Nakano A and Vashishta P 2006 *Phys. Rev. Lett.* **96** 065502
[48] Branicio P S, Kalia R K, Nakano A, Vashishta P, Shimojo F and Rino J P 2008 *J. Mech. Phys. Solids* **56** 1955
[49] Zhang C, Kalia R K, Nakano A and Vashishta P 2007 *Appl. Phys. Lett.* **91** 071906
[50] Zhang C, Kalia R K, Nakano A, Vashishta P and Branicio P S 2008 *J. Appl. Phys.* **103** 083508
[51] Vasil'ev V P and Gachon J C 2006 *Inorg. Mater.* **42** 1171
[52] Hohenberg P and Kohn W 1964 *Phys. Rev.* **136** B864
[53] Kohn W and Sham L J 1965 *Phys. Rev.* **140** A1133
[54] Kresse G and Furthmuller J 1996 *Phys. Rev.* B **54** 11169
[55] Vanderbilt D 1990 *Phys. Rev.* B **41** 7892
[56] Monkhorst H J and Pack J D 1976 *Phys. Rev.* B **13** 5188
[57] Tadmor E B and Hai S 2003 *J. Mech. Phys. Solids* **51** 765
[58] Suzuki T, Nishisako T, Taru T and Yasutomi T 1998 *Phil. Mag. Lett.* **77** 173
[59] Takeuchi S and Suzuki K 1999 *Phys. Status Solidi* a **171** 99
[60] Touloukian Y S and Buyco E H 1970 *Specific Heat: Nonmetallic Solids* (New York: IFI/Plenum) p xxx
[61] Kagaya H M and Soma T 1986 *Phys. Status Solidi* b **134** K101
[62] Nye J F 1984 *Physical Properties of Crystals: Their Representation by Tensors and Matrices* (New York: Clarendon) (Oxford: Oxford University Press)
[63] Weiser K 1957 *J. Phys. Chem.* **61** 513
[64] Harrison W A 1989 *Electronic Structure and the Properties of Solids: the Physics of the Chemical Bond* (New York: Dover)
[65] Glazov V M, Davletov K, Nashelskii A Y and Mamedov M M 1977 *Zh. Fiz. Khim.* **51** 2558
[66] Nichols D N, Rimai D S and Sladek R J 1980 *Solid State Commun.* **36** 667
[67] Hickerne F S and Gayton W R 1966 *J. Appl. Phys.* **37** 462